

Crystalline Order on Catenoidal Capillary Bridges

Mark J. Bowick and Zhenwei Yao

Department of Physics, Syracuse University, Syracuse, New York 13244-1130, USA

We study the defect structure of crystalline particle arrays on negative Gaussian curvature capillary bridges with vanishing mean curvature (catenoids). The threshold aspect ratio for the appearance of isolated disclinations is found and the optimal positions for dislocations determined. We also discuss the transition from isolated disclinations to scars as particle number and aspect ratio are varied.

PACS numbers: 61.72.Lk Linear defects: dislocations, disclinations

Two-dimensional ordered phases of matter on spatially curved surfaces have several features not found in the corresponding phase for planar or flat space systems [1]. For crystalline order on surfaces of spherical topology where disclination defects are required by the topology itself, Gaussian curvature can drive the sprouting of disclination defects from point-like structures to linear grain boundary scars which freely terminate in the crystal [2–5]. Even for surfaces such as the torus which admit completely defect-free crystalline lattices, the energetics in the presence of Gaussian curvature can favor the appearance of isolated disclination defects in the ground state [6, 7]. For the axisymmetric torus with aspect ratio between 4 and 10, isolated 5-fold disclinations appear near the line of maximal positive Gaussian curvature on the outside and isolated 7-fold disclinations appear near the line of maximal negative Gaussian curvature on the inside [8]. The ground states in these systems are thus distinguished by a defect structure that would be energetically prohibitive in flat space. It is certainly worthwhile to explore as many settings as possible in which there are qualitative changes in the fundamental structure of the ground state, within a given class of order, purely as a consequence of spatial curvature.

The richest confluence of theoretical and experimental ideas in the area of curved two-dimensional phases of matter has been in colloidal emulsion physics in which colloidal particles self-organize at the interface of two distinct liquids, either in particle-stabilized (Pickering) emulsions [9, 10] or charge-stabilized emulsions [11, 12]. Two-dimensional (thin-shell) spherical crystals form at the surface of droplets held almost perfectly round by surface tension. The ordered configurations of particles may be imaged with confocal microscopy and the particles manipulated with optical tweezers [5, 13, 14]. Macroscopic examples of crystalline order on variable positive Gaussian curvature surfaces have been constructed by forming a soap bubble raft on a spinning liquid [15] and the nature of the order has been analyzed theoretically [16].

Glassy liquids on negative Gaussian curvature manifolds have also received considerable attention [17–21]. The simplest such manifold conceptually is the constant (negative) curvature hyperbolic plane H^2 and it even appears that the hyperbolic plane can be isometrically

embedded as a complete subset of Euclidean 3-space, although not differentiably [22]. Physical realizations of negative Gaussian curvature manifolds in condensed matter physics will almost always have variable Gaussian curvature. The inner wall of the axisymmetric torus ($S^1 \times S^1$) has integrated Gaussian curvature equal to -4π , balancing an equal and opposite integrated Gaussian curvature on the outer wall. This is responsible for the novel ground states noted above. Gaussian bumps have regions of both positive and negative Gaussian curvature and the minimal-type surfaces found in bicontinuous phases of amphiphilic bilayers have spatially extended variable Gaussian curvature that is negative on average [23].

Recently crystalline particle arrays on variable Gaussian curvature surfaces has been studied by assembling particles on capillary bridges formed by glycerol in bulk oil spanning two flat parallel plates [24]. Configurations may be imaged by confocal microscopy and even manipulated with laser tweezers. The interface between the inner fluid of the capillary bridge and the outer bulk fluid is a surface of revolution with a constant mean curvature (CMC) determined by the pressure difference between the two fluids [25, 26]. Capillary bridges minimize the surface area at fixed volume and perimeter and appear in the classical work of Delaunay [27, 28]. The value of the mean curvature and hence the underlying surface may be changed by varying the spacing between the plates.

Three classes of the Delaunay surfaces have negative Gaussian curvature - the nodoids, unduloids and catenoids. We will focus on the most analytically tractable case of a catenoidal capillary bridge in which the mean curvature is everywhere zero. Capillary bridges themselves have wide-ranging application. They play an essential role in adhesion, antifoaming, the repelling coffee-ring effect and in the origin of attractive hydrophobic forces [29–32].

The shape of a capillary bridge with mean curvature H follows by solving

$$2H = \frac{-r''}{(1+r'^2)^{3/2}} + \frac{1}{r\sqrt{1+r'^2}} = \text{const.}, \quad (1)$$

where $2H \equiv \frac{1}{R_1} + \frac{1}{R_2}$, $r = r(z)$ is the representation of a surface of revolution with symmetry axis z and R_1 and R_2 are the two principal radii of curvature at any point.

The solution corresponding to the special case $H = 0$ (a minimal surface) is

$$\vec{x}(u, v) = \begin{pmatrix} c \cosh(\frac{v}{c}) \cos u \\ c \cosh(\frac{v}{c}) \sin u \\ v \end{pmatrix}, \quad (2)$$

where $u \in [0, 2\pi)$ and $v \in (-z_m, z_m)$. This surface is the well-known *catenoid* parameterized by the radius of the waist c located in the $z = 0$ plane (see Fig.1). From the non-zero metric components $g_{uu} = c^2 \cosh^2(\frac{v}{c})$ and $g_{vv} = \cosh^2(\frac{v}{c})$, one can obtain the Gaussian curvature $K \equiv \frac{1}{R_1} \frac{1}{R_2} = -\frac{1}{c^2} \text{sech}^4(\frac{v}{c}) = -\frac{1}{g}$, where g is the determinant of the metric tensor. We see explicitly that the metric completely determines the Gaussian curvature. The solution to Eq.(1) for $H \neq 0$ is [33]

$$\vec{x}(u, t) = \begin{pmatrix} \gamma \Delta(\theta, t) \cos u \\ \gamma \Delta(\theta, t) \sin u \\ \alpha + \gamma(E(\theta, t) + F(\theta, t) \cos \theta) \end{pmatrix}, \quad (3)$$

where $t \in [t_0, t_1]$, $u \in [0, 2\pi)$, $E(\theta, t) = \int_0^t \Delta(\theta, \tilde{t}) d\tilde{t}$, $F(\theta, t) = \int_0^t 1/\Delta(\theta, \tilde{t}) d\tilde{t}$ and $\Delta(\theta, t) = \sqrt{1 - \sin^2 \theta \sin^2 t}$. γ plays the role of a scale factor. The curves generated are periodic in t with period π and have maxima at $t = k\pi$ and minima at $t = (k + 1/2)\pi$ for integer k . The value of θ controls the shape of the profile: it generates an unduloid for $\theta \in [0, \pi/2)$, a nodoid for $\theta \in (\pi/2, \pi)$; and a semi-circle for $\theta = \pi$. The shapes of the capillary bridges in the work of [24] can be fit by Eq.(3), the general CMC expression with $H \neq 0$.

Here we study crystalline order on the simplest case of a catenoidal capillary bridge ($H = 0$) in the framework of continuum elasticity theory [1, 2, 34]. For simplicity, we measure all lengths in units of the radius of the contact disk.

The topology of the capillary surfaces we study is that of the annulus, with Euler characteristic zero, since the liquid bridge makes contact with the plates at the top and bottom. Such a surface admits regular triangulations with all particles having coordination number 6. Although defects (non 6-fold coordinated particles) are not topologically required they may be preferred in the crystalline ground state for purely energetic reasons since negative Gaussian curvature will favor the appearance of 7-coordinated particles (-1 disclinations). To determine the preferred defect configuration we map the microscopic interacting particle problem to the problem of discrete interacting defects in a continuum elastic background. The defect free energy F_{el} , in the limit of vanishing core energies, may be expressed in the form [1, 16]

$$F_{el} = \frac{1}{2} Y \int_M G_{2L}(\vec{x}, \vec{y}) \rho(\vec{x}) \rho(\vec{y}) d^2 \vec{x} d^2 \vec{y}. \quad (4)$$

Here $G_{2L}(\vec{x}, \vec{y})$ is the Green's function for the covariant biharmonic operator on the surface M , Y is the Young's modulus for the crystalline packing, and \vec{x} and \vec{y} are position vectors on the surface. The effective topological

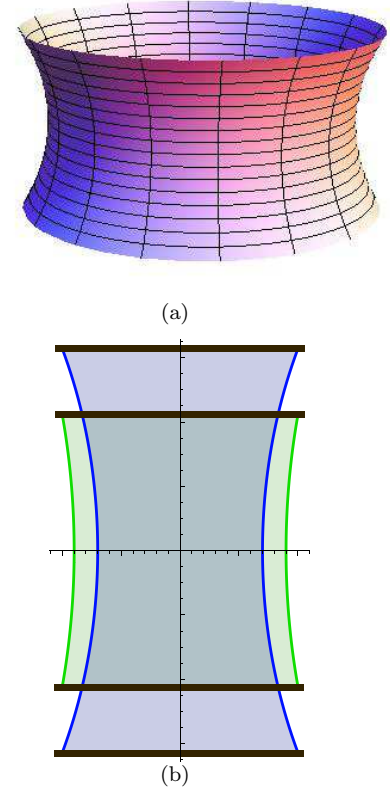


FIG. 1: (a) The three dimensional shape of a catenoid with aspect ratio $c = 0.85$. (b) A catenoid with aspect ratio $c = 0.9$ (green) deforms to $c = 0.7$ (blue).

charge density is $\rho(\vec{x}) = \frac{\pi}{3} q(\vec{x}) - \gamma^{ij} \nabla_j b_i(\vec{x}) - K(\vec{x})$, in which the first term is the disclination charge density $q(\vec{x}) = \sum_\alpha q_\alpha \delta(\vec{x} - \vec{x}_\alpha)$, the second term is the dislocation density $b_i(\vec{x}) = \sum_\beta b_i^\beta \delta(\vec{x} - \vec{x}_\beta)$ and $K(\vec{x})$ is the Gaussian curvature. In this expression $\gamma^{ij} = \epsilon^{ij} / \sqrt{g}$. By introducing χ and Γ such that $\Delta^2 \chi(\vec{x}) = Y \rho(\vec{x})$ and $\Gamma(\vec{x}) = \Delta \chi(\vec{x})$, Eq.(4) can be written in a more compact form

$$F_{el} = \frac{1}{2Y} \int_M \Gamma^2(\vec{x}) d\vec{x}, \quad (5)$$

in which $\Gamma(\vec{x})/Y = \int G_L(\vec{x}, \vec{y}) \rho(\vec{y}) d\vec{y} + U(\vec{x})$ with $\Delta U(\vec{x}) = 0$ and $G_L(\vec{x}, \vec{y})$ is the Green's function for the covariant Laplacian on M which satisfies $\Delta G_L(\vec{x}, \vec{y}) = \delta(\vec{x}, \vec{y})$; $\vec{x}, \vec{y} \in M$ with the boundary condition $G_L(\vec{x}, \vec{y}) = 0$; $\vec{x}, \vec{y} \in \partial_M$. By conformally mapping the surface parameterized by $\{u, v\}$ onto an annulus in the complex plane via $z = \rho(u, v) e^{iu}$, the Green's function G_L is found to be [16] $G_L(\vec{x}, \vec{y}) = \frac{1}{2\pi} \ln |(\rho_0^{-1} z(\vec{x}) - z(\vec{y})) / (1 - \rho_0^{-1} z(\vec{x}) \bar{z}(\vec{y}))|$, in which ρ_0 is the radius of the outer circle of the annulus in the complex plane. For a catenoid, the conformal mapping is given by $\rho(u, v) = c e^{|v|/c}$ and $\rho_0 = c \exp(\text{arcsech}(c))$.

Disclinations are expected to appear in the crystalline ground state when the Gaussian curvature is sufficient to support them. Consider therefore a putative isolated

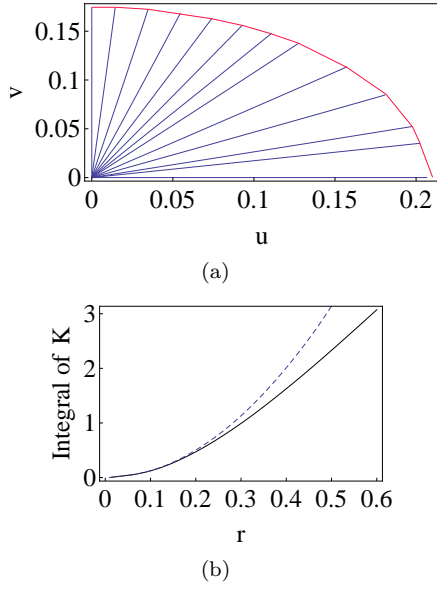


FIG. 2: (a) A family of geodesics in $\{u, v\}$ coordinates centered at a point on the waist of a catenoid with $c = 0.85$. (b) The $|K(0)|\pi r^2$ (dashed curve) and numerical result (solid curve) of the integrated Gaussian curvature over a geodesic disk of radius r versus r . $c = 1/2$.

disclination of strength $q = -1$ (coordination number 7) at the waist of a catenoid. The curvature condition above requires that there exist a disk of geodesic radius r_c , centered on the 7-disclination, for which [1, 24]

$$\int_{disk} K dA = -\frac{\pi}{3}. \quad (6)$$

Clearly r_c must be less than the geodesic distance l from the waist to the boundary [24]. For a given size catenoid c , we calculate l and the integral of the Gaussian curvature over the geodesic disk of radius l . The value of c for which the integrated curvature equals $-\pi/3$ is the critical value of c for the appearance of 7-disclinations. We compute the integral of the Gaussian curvature numerically. We first construct a family of geodesics radiating from the core 7-disclination (at $u = 0, v = 0$) by solving the geodesic equation:

$$\frac{d^2 x^\mu}{d\lambda^2} + \Gamma_{\rho\delta}^\mu \frac{dx^\rho}{d\lambda} \frac{dx^\delta}{d\lambda} = 0, \quad (7)$$

in which $x^1 = u, x^2 = v$ and $\Gamma_{\rho\delta}^\mu$ is the Christoffel symbol of the second kind. This second order differential equation has a unique solution given an initial position and an initial velocity. The initial conditions are $x^1(0) = x^2(0) = 0$, $\frac{dx^1}{d\lambda}|_0 = \frac{1}{c} \cos \theta$, and $\frac{dx^2}{d\lambda}|_0 = \sin \theta$, where θ is the angle of the initial velocity with respect to \vec{e}^u . Given a geodesic radius r , the coordinates of the end point of the geodesic curve can be found. These end points form the boundary of a disk in $\{u, v\}$ coordinates (see Fig.2(a)). We then integrate the Gaussian curvature over the prescribed disk numerically. The critical

value of c is found to be $c^* = 0.85$ and the corresponding critical radius is $r_c = 0.53$. Note that integrated Gaussian curvature for this critical catenoid is quite large [24]: $\int K dA = -6.6$. The critical value c^* can also be estimated as follows. By introducing Gaussian normal coordinates (r, θ) centered on a 7-disclination at height z_0 above or below the waist of the catenoid, the effective (screened) disclination charge at distance r is given by [2, 35]

$$\begin{aligned} \rho_{eff}(r) &= -\frac{\pi}{3} - \int_0^{2\pi} d\theta \int_0^r dr' \sqrt{g} K(r') \\ &= -\frac{\pi}{3} + \pi \frac{r^2}{c^2} \text{sech}^4\left(\frac{z_0}{c}\right) + \mathcal{O}(r^3). \end{aligned} \quad (8)$$

The critical radius is reached when the effective disclination density vanishes: $\rho_{eff}(r_c) = 0$. For a 7-disclination on the waist ($z_0 = 0$) this gives $r_c/c \equiv \theta_c = \sqrt{1/3} \approx 33^\circ$. Now on the catenoid the geodesic length from the waist to the boundary is $\int_0^{z_m} \cosh(v/c) dv = \sqrt{1-c^2}$. The critical catenoid size c^* is then given by $r_{c^*} = \sqrt{1-c^{*2}}$. This yields $c^* = \sqrt{3}/2 \approx 0.87$. This estimate for c^* is very close to the numerical value 0.85. Why are these two values so close? In calculating the effective disclination charge, we use $K(0)\pi r^2$ to approximate the integral of the Gaussian curvature over a geodesic disk of radius r . The Gaussian curvature is overestimated as its magnitude is maximum at $r = 0$ (on the waist). On the other hand, since $K(0) = \lim_{r \rightarrow 0} \frac{12}{\pi r^4} (\pi r^2 - A(r)) < 0$, the real area $A(r)$ of the disk with geodesic radius r is bigger than πr^2 , i.e., the disk area is underestimated in our approximation. These two approximations tend to cancel each other out. For a typical value of $c = 1/2$, $|K(0)|\pi r^2$ and the numerical result of the integral of the Gaussian curvature versus r is plotted in Fig.2(b). As expected the flat space approximation $K(0)\pi r^2$ is good for small r ($r < 0.2$).

The critical waist size c^* can also be estimated from energetic arguments. From the free energy of Eq.(5) one can analyze the geometric potential describing the interaction between disclinations and the intrinsic Gaussian curvature of the surface. The result is shown in Fig.3). We see that the optimal position of a disclination shifts from the boundary to the waist as c decreases. The transition point for the emergence of a disclination in the interior of a catenoidal capillary bridge is $c^* \approx 0.8$, again consistent with the value obtained above based on geometrical arguments.

Net disclination charges may appear either in the form of point-like isolated disclinations or extended linear grain boundary scars. Scars result from the screening of an isolated disclination by chains of dislocations and typically arise when the number of particles exceeds a threshold value beyond which the energy gained exceeds the cost of creating excess defects [1]. Here we semi-quantitatively construct the phase diagram for isolated disclinations versus scars on a catenoidal capillary bridge characterized by the number of particles and the aspect ratio of the catenoid c .

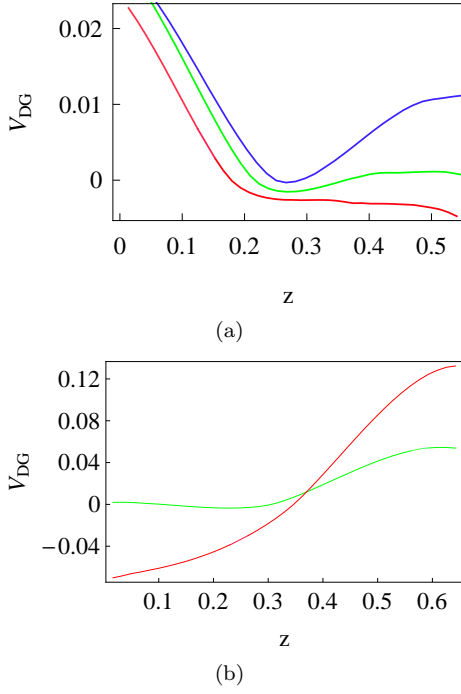


FIG. 3: (a) The geometric potential of an isolated disclination for three different values of c : $c = 0.8$ (red), $c = 0.75$ (green) and $c = 0.7$ (blue). The optimal position of an isolated disclination moves from the boundary to the waist of the catenoid in the rather narrow window c between 0.8 and 0.75. (b) The geometric potential of an isolated disclination for catenoids with $c = 0.5$ (red) and $c = 0.6$ (green).

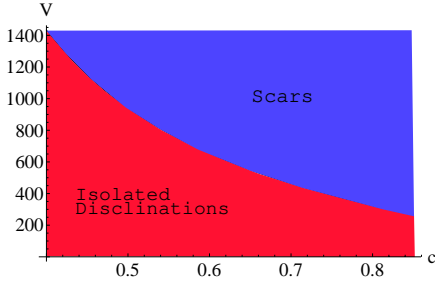


FIG. 4: The phase diagram in the particle number-aspect ratio plane for isolated disclinations versus scars for $c < c^*$.

Consider a disclination on a capillary bridge (for $c < 0.85$) radiating m grain boundaries (scars). The spacing of neighboring dislocations is $l = a m/s_{eff}$ [2], where a is the lattice spacing. As $s_{eff} \rightarrow 0$, the dislocation spacing within a scar diverges and the grain boundary terminates. If the disclination can be completely screened by Gaussian curvature within a circle of radius $r \approx 3a$, then grain boundaries will not form around the core disclination. The condition for isolated disclinations is therefore $|K_{max}\pi(3a)^2| \sim \pi/3$, where $|K_{max}| = 1/c^2$ is the Gaussian curvature at the waist of the bridge. On the other hand, the number of particles N is related to the surface area A between $z \in [-z_m, z_m]$ via $A(c) = \frac{\sqrt{3}}{2}a^2N$.

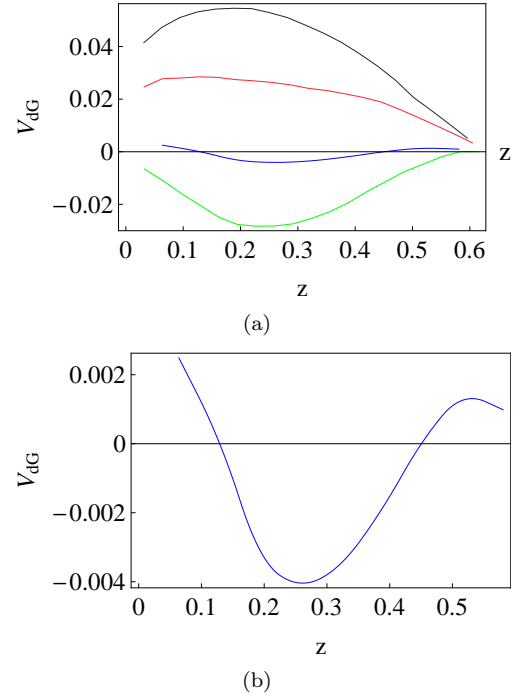


FIG. 5: (a) The geometric potential of isolated dislocations as a function of height for four different values of c : $c = 0.7$ (black), $c = 0.68$ (red), $c = 0.66$ (blue) and $c = 0.65$ (green). The optimal position moves from near the boundary towards the waist as c decreases. (b) is an enlarged view of the blue curve to show the transition from the red to the green curve.

The curve separating isolated disclinations from scars is thus given by $N = \frac{18\sqrt{3}}{c^2} \frac{A(c)}{c^2}$, as plotted in Fig.4(a). The phase boundary reveals two basic types of transition in the topological structure of the ground state as the particle number and the geometry (aspect ratio) of the capillary bridge are varied. For a fixed catenoid aspect ratio below the critical value for the appearance of excess 7s in the interior there is a transition from isolated 7s to linear grain boundary scars with one excess 7 as the number of particles increases. For a fixed number of particles above a threshold value ($N_c \approx 300$) there is a transition from isolated disclinations to scars as the capillary bridge gets fatter and the decreasing Gaussian curvature is insufficient to support isolated 7-disclinations.

Disclinations and anti-disclinations attract and may form dipole bound states (7-5 pairs). Such dipole configurations are themselves another type of point-like topological defect in two-dimensional crystals - dislocations. Dislocations on a triangular lattice correspond to two semi-infinite Bragg rows 60° apart both terminating at a common point - the location of the dislocation. Since they are tightly bound states of disclinations the energetics of dislocations may be derived from the governing energetics of disclinations on a curved geometry - Eq.(5). Dislocations, unlike disclinations, are oriented. The Burgers vector \vec{b}^α characterizing a dislocation at po-

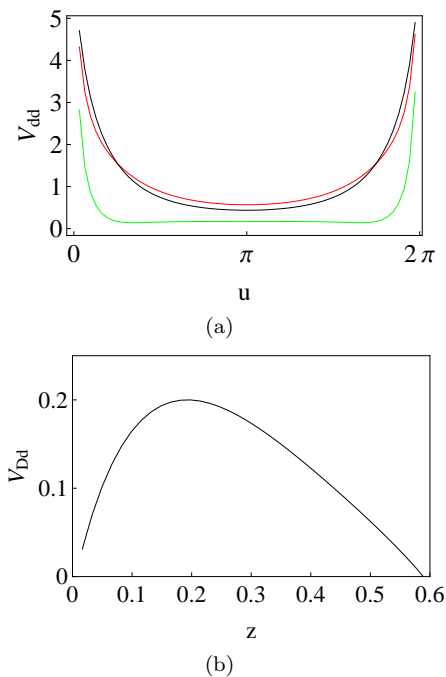


FIG. 6: The interaction of defects. (a) The dislocation-dislocation interaction V_{dd} of two dislocations along \vec{e}^u at the same height. $z = 0.5 z_m$ (black), $z = 0.3 z_m$ (red) and $z = 0.1 z_m$ (green). (b) The disclination-dislocation interaction V_{Dd} as a function of their longitudinal separation. The disclination is fixed on the waist ($c = 1/2$).

sition x^α is perpendicular to the 5-7 bond. An analysis of Eq.(5) shows that the preferred orientation of the Burgers vector is along \vec{e}^u . This is clear from the fact that the 7-disclination has minimum energy when located at the waist with the accompanying 5-disclination in the direction of the boundary where the negative Gaussian curvature drops most rapidly. Thus the 7-5 bond should along a meridian and the Burgers vector along a line of latitude. From here on we restrict ourselves to this case.

The variable Gaussian curvature of a catenoidal capillary bridge also leads to optimal positions for isolated dislocations. Fig.5 shows the geometric potential for isolated dislocations as a function of height above the waist. As the waist radius c decreases the optimal position of an isolated dislocation moves from the boundary to the interior of the capillary bridge since the increasing maximal negative Gaussian curvature increas-

ingly attracts 7-disclinations with their tightly bound 5-disclinations. The boundary-to-interior transition occurs for $c^{**} \approx 0.68$. The corresponding integrated Gaussian curvature $\int K dA \approx -9.0$ [24]. This detachment transition is also observed in experiments with capillary bridges [24] - in the experimental case the capillary bridges are generally nodoids with non-vanishing mean curvature and the analysis is corresponding more elaborate. The optimal position of a single dislocation for small c , say $c = 0.3$, is $z(c = 0.3) = 0.25 z_m$. Thus the optimal position of a single dislocation is far from the waist, even for a strongly curved catenoidal capillary bridge, in contrast to the case of disclinations. This result can be understood in terms of the Peach-Koehler forces acting on the individual positive and negative disclinations that make up a dislocation [24, 36]. While the 7-disclination prefers to be at the waist the 5 prefers to be at the boundary - the competition results in an optimal dislocation position somewhere in between the two extremes. Here we treat only single dislocations but it is possible for chains of dislocations to appear in the form of pleats, as elegantly discussed in Ref.[24].

Finally we turn to the interaction between defects themselves. Fig.6 (a) shows the dislocation-dislocation interaction along \vec{e}^u . Two dislocations at the same height feel a short-range repulsion. Note that near the waist shallow local minima appear. This differs from the interaction in flat space where parallel dislocations always repel to each other with a logarithmic potential [37]. The attractive interaction between a disclination and a nearby dislocation is shown in Fig.6(b) with the disclination fixed on the waist.

The influence of spatial curvature and topology on two-dimensional phases of matter continues to yield surprises. The presence of 7-disclinations in negative curvature crystals may offer unique opportunities for functionalization of micron-scale crystallized "superatoms" via chemistry that recognizes the unique crowded environment of a 7-disclination [1, 38].

Acknowledgements

We thank William Irvine, Paul Chaikin and David Nelson for discussions. This work was supported by the National Science Foundation grant DMR-0808812 and by funds from Syracuse University.

-
- [1] M.J. Bowick and L. Giomi, Adv. Phys. **58**, 449 (2009) [arXiv:0812.3064].
 - [2] M.J. Bowick, D.R. Nelson and A. Travesset, Phys. Rev. B **62**, 8738 (2000) [arXiv:cond-mat/9911379].
 - [3] M.J. Bowick, A. Cacciuto, D.R. Nelson, and A. Travesset, Phys. Rev. Lett. **89**, 185502 (2002) [arXiv:cond-mat/0206144].
 - [4] M.J. Bowick, A. Cacciuto, D.R. Nelson and A. Travesset, Phys. Rev. B **73**, 024115 (2006) [arXiv:cond-mat/0509777].
 - [5] A.R. Bausch *et al.*, Science **299**, 1716 (2003) [arXiv:cond-mat/0303289].
 - [6] L. Giomi and M.J. Bowick, Phys. Rev. E **78**, 010601(R) (2008) [arXiv:0801.3484].

- [7] L. Giomi and M.J. Bowick, Eur. Phys. J. E **27**, 275 (2008) [arXiv:0807.4538].
- [8] L. Giomi and D. Giuliani, <http://physics.syr.edu/~lgiomi/torus/database/>.
- [9] S. Pickering, J. Chem. Soc. **91**, 2001 (1907).
- [10] *Colloidal Particles at Liquid Interfaces*, Themed Issue, ed. B.P. Binks, Phys. Chem. Chem. Phys. **9**, 6285-6488 (2007).
- [11] M.E. Leunissen, A. van Blaaderen, A.D. Hollingsworth, M.T. Sullivan and P.M. Chaikin, Proc. Nat. Acad. Sci. USA **104**, 2585 (2007).
- [12] M.E. Leunissen, J. Zwanikken, R. van Roij, P.M. Chaikin and A. van Blaaderen, Phys. Chem. Chem. Phys. **9**, 6405 (2007).
- [13] A.D. Dinsmore et al; Science **298**, 1006 (2002).
- [14] W.T.M. Irvine, A.D. Hollingsworth, D.G. Grier and P.M. Chaikin, *Topological tweezers*, submitted to Proc. Nat. Acad. Sci. (2010).
- [15] M.J. Bowick, L. Giomi, H. Shin and C.K. Thomas, Phys. Rev. E **77**, 021602 (2008) [<http://arxiv.org/abs/0709.2731v1>].
- [16] L. Giomi and M.J. Bowick, Phys. Rev. B **76**, 054106 (2007) [arXiv:cond-mat/0702471].
- [17] G. Tarjus, F. Susset and P. Viot, *Statistical Mechanics of liquids and fluids in curved space*, submitted to Adv. Chem. Phys. [<http://arxiv.org/abs/1005.2684v1>].
- [18] M. Rubinstein and D.R. Nelson, Phys. Rev. B **28**, 6377 (1983).
- [19] F. Sausset, G. Tarjus and D.R. Nelson, Phys. Rev. E **81**, 031504 (2010) [arXiv:0911.0387].
- [20] C.D. Modes and R.D. Kamien, Phys. Rev. Lett. **99**, 235701 (2007) [arXiv:0810.5724].
- [21] C.D. Modes and R.D. Kamien, Phys. Rev. E **77**, 041125 (2008) [arXiv:0801.1166].
- [22] D.W. Henderson and D. Taimina, Math. Intell. **23** (2) 17 (2001).
- [23] J.F. Sadoc and J. Charvolin, Acta. Cryst. A, **45**, 10 (1989).
- [24] W.T.M. Irvine, V. Vitelli and P.M. Chaikin, Nature **468**, 947 (2010).
- [25] P.G.de Gennes, F. Brochard-Wyart and D. Quéré, *Capillarity and Wetting Phenomena: Drops, Bubbles, Pearls, Waves*, (Springer, New York, 2003).
- [26] <http://www.gang.umass.edu/>.
- [27] J. Eells, Math. Intell. **9**, 53 (1987).
- [28] C. Delaunay, J. Math. pures et appl. **Sér. 1 (6)**, 309 (1841).
- [29] B.K. Weon and J.H. Je, Phys. Rev. E **82**, 015305 (2010).
- [30] N.D. Denkov and P.A. Kralchevsky, Curr. Opin. Coll. Int. Sci. **6**, 383 (2001).
- [31] K. Nagayama and P.A. Kralchevsky, Adv. Coll. Int. Sci. **85**, 145 (2000).
- [32] R.D. Deegan et al., Nature **389**, 827 (1997).
- [33] R.D. Gillette and D.C. Dyson, Chem. Eng. **2**, 44 (1971).
- [34] D.R. Nelson and L. Peliti, J. Phys. (France) **48**, 1085 (1987).
- [35] T. Frankel, *The Geometry of Physics, An Introduction* (Cambridge Press, second edition, 1997).
- [36] V. Vitelli, J.B. Lucks, and D.R. Nelson, PNAS **103**, 12323 (2006) [arXiv:cond-mat/0604203].
- [37] J. Weertman and J.R. Weertman, *Elementary Dislocation Theory* (The Macmillan Company, 1964).
- [38] G.A. DeVries et al., Science **315**, 358 (2007).